ChemComm

COMMUNICATION

View Article Online
View Journal | View Issue

Cite this: *Chem. Commun.*, 2025, **61**, 6178

Received 16th February 2025,
Accepted 24th March 2025

DOI: 10.1039/d5cc00860c

rsc.li/chemcomm

Terminal hydride formation in [FeFe] hydrogenase: understanding the role of the dithiolate bridgehead†

Anjali Depala,[a] Manon T. Lachmann,[b] Simone Morra,[c] James A. Birrell *[d] and Patricia Rodríguez-Maciá *[b]

[FeFe]-hydrogenases are highly-active hydrogen-conversion biocatalysts using Earth-abundant metals in their active-site. Understanding their mechanism may enable design of catalysts for renewable energy storage. Here, observation of the crucial Fe-hydride-containing (H_{hyd}) intermediate in a PDT-variant of [FeFe]-hydrogenase reveals deeper insight into the role of the dithiolate bridgehead in the catalytic mechanism.

Fossil fuel utilisation has led to a surge in atmospheric carbon dioxide (CO_2), contributing to climate change.[1] We urgently need to transition to renewable energy and find new methods to produce fossil fuel derived chemical precursors. A major challenge is that the currently available catalysts for hydrogen (H_2) production are based on precious metals such as platinum or display poor activity and efficiency.[2–4] Therefore, we must develop new catalysts using Earth-abundant metals like iron. Nature offers inspiration in the form of hydrogenases: highly active and reversible enzymes for H_2 production and oxidation.[5] Among the three phylogenetic classes of hydrogenases, [FeFe] hydrogenases are the most active and reversible and, therefore, of greatest technological interest. Their active site is based on Fe, and they achieve catalytic performances comparable to platinum.[6] A deeper understanding of [FeFe] hydrogenases' mechanisms would provide additional design criteria for building new, efficient and affordable catalysts enabling renewable energy storage in the form of H_2.

The active site, known as the H-cluster (Fig. 1A), consists of a canonical [4Fe–4S] cluster ($[4Fe–4S]_H$) covalently attached, through the thiolate group of a cysteine amino-acid residue, to a unique [2Fe] site ($[2Fe]_H$), where catalysis occurs.[7–9] $[2Fe]_H$ comprises two Fe ions, the proximal Fe (Fe_p), which is closest to $[4Fe–4S]_H$, and the distal Fe (Fe_d), bridged by a CO and a unique 2-azapropane-1,3-dithiolate (ADT) ligand. Each iron is also coordinated to a terminal CO and a terminal CN^- ligand. This leaves an open coordination site on Fe_d for binding H_2.

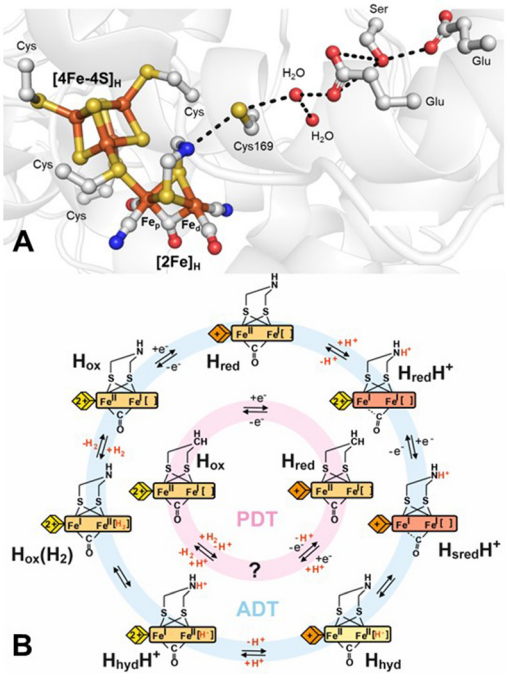

Fig. 1 (A) Structure around the H-cluster based on PDB ID 4XDC.[11] Cys169 (CrHydA1 nomenclature) of the proton-transfer pathway is labelled along with cysteines ligating the H-cluster and the key amino acids of the proton-transfer pathway. (B) Proposed catalytic cycle for the native ADT ligand-containing H-cluster (blue) and the semi-synthetic PDT ligand-containing H-cluster (pink). The yellow/orange diamond represents $[4Fe–4S]_H$ in the 2+ and 1+ states, respectively, while the yellow/orange/red rectangle represents $[2Fe]_H$ in the $Fe_p(II)Fe_d(II)$, $Fe_p(II)Fe_d(I)$ and $Fe_p(I)Fe_d(I)$ states, respectively. Terminal CO/CN^- ligands are omitted for clarity.

[a] *Department of Chemistry, University of Oxford, Inorganic Chemistry laboratory, South Parks Road, Oxford, OX1 3QR, UK*
[b] *School of Chemistry and Leicester Institute for Structural and Chemical Biology, University of Leicester, University Road, Leicester, LE1 7RH, UK. E-mail: prm28@leicester.ac.uk*
[c] *University of Nottingham, Faculty of Engineering, Coates Building, University Park, Nottingham, NG7 2RD, UK*
[d] *School of Life Sciences, University of Essex, Wivenhoe Park, Colchester, CO4 3SQ, UK. E-mail: james.birrell@essex.ac.uk*

† Electronic supplementary information (ESI) available. See DOI: https://doi.org/10.1039/d5cc00860c

This arrangement of ligands results in the formation of a frustrated Lewis pair (FLP),[10] with the open coordination site on Fe_d acting as a Lewis acid to bind H_2 and the NH group of the dithiolate ligand serving as a base. This FLP arrangement polarises the H–H bond to facilitate heterolytic splitting by abstraction of a proton by the NH base as well as through the stabilisation of a terminal hydride by the Fe_d Lewis acid.

The coordination of the Fe ions by strong-field CO and CN^- ligands stabilises low oxidation and low spin states, tuning the electronic structure of the H-cluster for catalytic activity. Both Fe ions can adopt either Fe(II) or Fe(I) oxidation states. $[4Fe–4S]_H$ is also redox-active and can alternate between $[4Fe–4S]^{2+}$ and $[4Fe–4S]^{1+}$ oxidation states. The ''resting'' state of the H-cluster, prior to reduction or binding of H_2, termed H_{ox}, has an oxidised $[4Fe–4S]_H$ and a mixed valent $Fe_p(II)Fe_d(I)$ $[2Fe]_H$. During proton reduction (Fig. 1B), the H_{ox} state is thought to become reduced by one electron on $[4Fe–4S]_H$, forming the H_{red} state. Protonation of the ADT ligand at the amine bridgehead results in the $H_{red}H^+$ state in which an electron has been transferred from $[4Fe–4S]_H$ to $[2Fe]_H$ generating an $Fe_p(I)Fe_d(I)$ $[2Fe]_H$.[12] This transfer makes $[4Fe–4S]_H$ available for a second reduction, leading to the formation of the $H_{sred}H^+$ state.[13] $H_{sred}H^+$ can tautomerise to yield a state in which a terminal hydride (H^-) forms on Fe_d, referred to as H_{hyd} (also $H_{hyd:red}$).[14–17] To form the terminal hydride, a proton from the bridging ammonium (NH_2^+) of the protonated ADT cofactor is transferred to Fe_d, causing one-electron oxidation of both Fe_p and Fe_d, yielding a $Fe(II)Fe(II)–H^-$ state. Further protonation of the ADT ligand is then thought to trigger electron transfer from $[4Fe–4S]_H$ to $[2Fe]_H$ in the $H_{hyd}H^+$ state. This state would have the ideal configuration for protonation of the terminal hydride to generate a H_{ox} state with H_2 bound. The final stages of catalysis have not yet been experimentally elucidated, and detailed structural, functional, and spectroscopic information is required for a more complete understanding of the catalytic cycle.[18]

H_{hyd} has a rich chemistry and hydride intermediates are crucial for activation of small molecules in metalloenzymes such as hydrogenases,[5] nitrogenases[19,20] and possibly CO dehydrogenases.[21] An important open question concerns the conditions under which the H_{hyd} state can be formed. In [FeFe] hydrogenases, this state was first observed in alanine (A, Ala)/serine (S, Ser) mutants of a cysteine adjacent to the ADT ligand of the proposed proton transfer pathway.[15,17,22] Later studies showed that a similar state could be formed in chemical variants of $[2Fe]_H$ in which the ADT ligand had been substituted with 2-oxapropane-1,3-dithiolate (ODT).[15,23,24] Another method for producing the H_{hyd} state in the native enzyme involved using high concentrations of the chemical reductant sodium dithionite (NaDT) at low pH.[15] The original explanation for the stabilisation of H_{hyd} in the C → A and C → S mutants and ODT variant was that they were all kinetically compromised for proton transfer. During H_2 oxidation, the deprotonation of H_{hyd} was slow, while during H_2 production, the protonation of H_{hyd} was slow. Following the same argument, low pH was proposed to inhibit the deprotonation of H_{hyd} during H_2 oxidation according to Le Chatelier's principle. However, H_{hyd} in the cysteine mutants and the ODT variant is thermodynamically stable (it is observed when the enzyme is incubated under H_2 in the absence of oxidants), and at low pH, dithionite stimulates H_2 production, not H_2 oxidation. Therefore, there is no reason to believe that the protonation of H_{hyd} during H_2 production would be slower at low pH – if anything, it should be faster. Instead, our hypothesis is that the variants and conditions that stabilise H_{hyd} achieve this by altering the electronic structure of the H-cluster, making the H_{hyd} state, with $Fe_p(II)Fe_d(II)–H^-$, more stable than the tautomeric $H_{sred}H^+$ state, with $Fe_p(I)Fe_d(I)–H^+$. The relative energies of $H_{sred}H^+/H_{hyd}$ were addressed previously using computational methods.[25–27] If the kinetic argument were correct, we would have expected the H-cluster variant containing a propane-1,3-dithiolate (PDT) ligand to behave identically to the ODT variant. However, reduction of the PDT variant with NaDT yields the H_{red} state, and H_{hyd} has not yet been observed in this variant.[28] Therefore, the open question is: why can't the PDT variant form the H_{hyd} state? We propose that it is not for kinetic but thermodynamic reasons and is just a matter of driving force.

While NaDT is already a strong reductant by biological standards ($E^\circ = -0.66$ V)[29] and has, for many reasons, become the reductant of choice for numerous enzymes, it is also known to form various products, some of which may interact directly with the enzyme of interest.[30] Therefore, in recent years, it has been proposed to use alternative low-potential reductants, including europium (II) complexes such as Eu(II)-diethylenetriamine pentaacetate (DTPA) ($E^\circ = -1.1$ V).[31–33] Vincent and colleagues were the first to utilise this complex in an enzyme, using it to reduce the Fe-protein of the nitrogenase.[33] Since then, Eu(II)-DTPA has been used to reduce iron–sulfur clusters in mitochondrial complex I.[31] Nevertheless, so far, Eu(II)-DTPA has not been utilised as a reductant for [FeFe] hydrogenases, but has been used with [FeFe] hydrogenase models.[34] Therefore, we investigated whether the PDT variant of [FeFe] hydrogenase could be reduced by Eu(II)-DTPA and whether this would trigger formation of the H_{hyd} state.

To this end, we used the model [FeFe] hydrogenase from *Chlamydomonas reinhardtii* (*Cr*HydA1), which contains only the active site H-cluster and lacks any additional redox cofactors (*e.g.* iron–sulfur clusters). This enzyme was prepared as previously described using heterologous expression in *Escherichia coli* and *in vitro* maturation with the synthetic PDT [2Fe] precursor.[23,35] Fig. 2 compares Fourier transform infrared (FTIR) spectra of *Cr*HydA1^{PDT} under various conditions (a) comparison of FTIR bands for *Cr*HydA1^{ADT}, *Cr*HydA1^{PDT} and *Cr*HydA1^{ODT} is provided in Fig. S1 (ESI†). Under as-isolated conditions (100% N_2), *Cr*HydA1^{PDT} is in the H_{ox} state (Fig. 2A) with IR bands at 2090, 2073, 1966, 1942 and 1811 cm^{-1}, almost identical to those reported previously.[28] In the presence of 10 mM NaDT, the sample converts to the H_{red} state (Fig. 2B) with IR bands (2085, 2067, 1964, 1935 and 1798 cm^{-1}) shifted to lower energy by an average of 7 cm^{-1} compared to H_{ox}. If, instead of NaDT, 10 mM Eu(II)-DTPA is added, the sample is converted to an entirely new state (Fig. 2C) where the IR bands (2089, 2072, 1977, 1961 and 1865 cm^{-1}) are shifted to higher energy, averaging 16 cm^{-1}

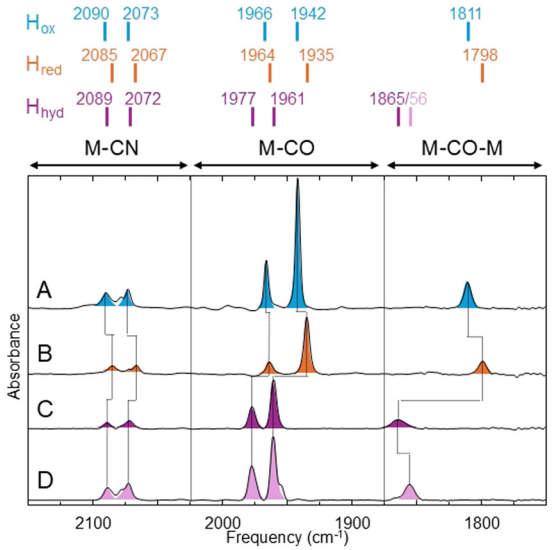

Fig. 2 IR spectra of *Cr*HydA1^{PDT} as isolated (A), reduced with sodium dithionite (B), and reduced with Eu(II)-DTPA in H_2O (C) and D_2O (D). The IR bands assigned to the H_{ox}, H_{red} and H_{hyd} states are coloured blue, orange and purple, respectively.

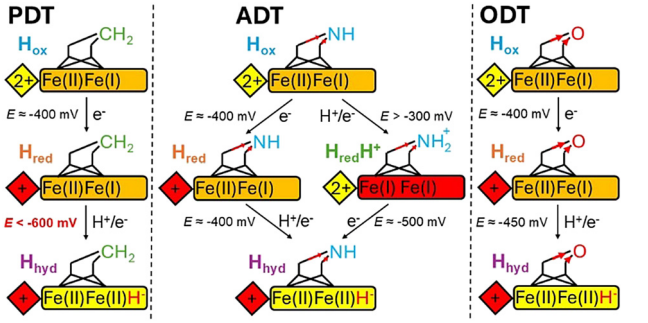

Fig. 3 Simplified representations of the H-cluster showing proposed pathways of H_{hyd} generation (see Fig. S6 for a more detail, ESI†). $[4Fe–4S]_H$ is shown as a diamond, $[2Fe]_H$ as a rectangle, the dithiolate ligand as sticks and the CO/CN are omitted. The native, ADT-containing enzyme in H_{ox} is doubly reduced (on $[4Fe–4S]_H$ and $[2Fe]_H$) and protonated at the ADT bridgehead yielding H_{hyd} *via* H_{red} or $H_{red}H^+$ intermediates. Both reduction steps happen with redox potentials close to −400 mV. For PDT and ODT, reduction of $[4Fe–4S]_H$ happens close to −400 mV (the dithiolate ligand has only a minor influence on the $[4Fe–4S]_H$ redox potential). Reduction of $[2Fe]_H$ in both the PDT and ODT cases proceeds without protonation of the dithiolate bridgehead, and the redox potential will depend on the stability of H_{hyd}. Electron withdrawal from the bridgehead group (O in ODT and CH_2 in PDT) is predicted to influence the electron density on the Fe ions with O more electron withdrawing than C. Hence, reduction of $[2Fe]_H$ and H_{hyd} formation occurs at less negative potentials in the ODT enzyme than in the PDT enzyme.

higher relative to H_{ox}, consistent with oxidation of $[2Fe]_H$ to a [Fe(II)Fe(II)] valence. The addition of a reductant leading to oxidation of $[2Fe]_H$ has so far only been observed when oxidative addition of a proton leads to terminal hydride formation on Fe_d.[17] To further investigate whether hydride formation had occurred in *Cr*HydA1^{PDT} on addition of Eu(II)-DTPA, we performed isotope-labelling experiments, in which the same experiment with *Cr*HydA1^{PDT} samples was performed in D_2O instead of H_2O. It has been previously observed that the bridging CO ligand IR stretch and the terminal Fe–H stretch are vibrationally coupled (the so-called "*trans*-effect"),[17] due to the Fe–H and bridging CO stretches having similar vibrational frequencies and optimal orbital overlap. Addition of Eu(II)-DTPA to *Cr*HydA1^{PDT} samples exchanged into D_2O buffer yielded a very similar state to that observed in H_2O buffer, except that the bridging CO IR band was shifted to lower energy by 9 cm^{-1} (Fig. 2D). This is expected since deuterium is heavier than hydrogen. All other bands had the same vibrational frequency in H_2O and D_2O. This is consistent with the presence of a terminal Fe–H/D on Fe_d.[17,24] The as-isolated enzyme in the presence of D_2O had an identical spectrum to that in H_2O (Fig. S3, ESI†).

Two variants of H_{hyd} have been proposed: $H_{hyd:ox}$, which contains an oxidised $[4Fe–4S]_H$, and $H_{hyd:red}$, which contains a reduced $[4Fe–4S]_H$.[14] We expect the H_{hyd} state formed under these conditions to be $H_{hyd:red}$. To classify the H_{hyd} state identified in *Cr*HydA1^{PDT}, we measured EPR spectra of Eu(II)-DTPA reduced *Cr*HydA1^{PDT} (Fig. S4, ESI†). Based on the electronic structure $H_{hyd:ox}$ is expected to be EPR silent while $H_{hyd:red}$ is expected to exhibit an EPR spectrum consistent with the reduction of a [4Fe–4S] cluster (rhombic $S = 1/2$ spectrum with $g_{av} \approx 1.9$). Eu(II)-DTPA reduced *Cr*HydA1^{PDT} shows a rhombic EPR spectrum with *g*-values of 2.073, 1.937 and 1.880 (Fig. S5, ESI†). This spectrum supports the hypothesis that the H_{hyd} state is $H_{hyd:red}$-like, with the EPR spectrum being very similar to that of the $H_{hyd:red}$ state of *Cr*HydA1^{ADT} (g = 2.069, 1.938, 1.880).[14]

Based on the results presented above, we can draw the following conclusions. The H_{hyd} state can be formed in the PDT variant of an [FeFe] hydrogenase but requires significantly more negative potentials ($E \ll -600$ mV) than those needed for the native ADT enzyme and the ODT variant (Fig. 3). These results do not align with a model that attributes the stabilisation of H_{hyd} in the ODT variant to kinetic reasons; rather, they are more consistent with a thermodynamic explanation. The ADT, PDT, and ODT ligands differ not only in their ability to undergo protonation at the central atom but also in their electronic structures. Oxygen is more electronegative than nitrogen, which is, in turn, more electronegative than carbon. Consequently, the thiolates of the PDT ligand are more electron-rich than those of ADT or ODT. This electron richness also influences the electron density of the Fe ions, which affects the redox potential of the $[2Fe]_H$ site. In all three variants, the reduction potential of $[2Fe]_H$ is too negative to be reduced without protonation[12] – protonation occurs either at the dithiolate bridgehead (for ADT only) or at Fe_d. This reduction potential is the least negative for the ODT variant but still requires protonation, which, due to the very low pK_a of the ether oxygen, can only occur at Fe_d, forming a terminal hydride. For the PDT variant, due to the inability to protonate a methylene group, reduction can likewise only occur at Fe_d, forming a terminal hydride. However, the redox potential is more negative than that of the ODT variant owing to the difference in electronegativity of the bridgehead atom. For the native ADT variant, the redox potential is between those of PDT and ODT, but the pK_a of the bridging amine is in the neutral

range,[12] making protonation more favourable on the amine than on Fe_d. Nevertheless, a tautomeric equilibrium exists in which the proton can be readily exchanged between the amine and metal. This equilibrium could explain the impressive activity and reversibility of [FeFe] hydrogenases and would explain why these properties are not observed in the active-site variants.

Overall, the results presented here highlight the crucial role that the dithiolate ligand plays in the [FeFe] hydrogenase, serving not only as a proton transfer relay that provides rapid proton transfer to and from Fe_d but also as a key player in tuning the electronic features of the diiron cofactor. This tuning is necessary to balance the requirement for stabilising terminal hydrides during H_2 oxidation without overly stabilising them and thereby limiting H_2 formation. This implies that ideal synthetic catalysts for reversible H_2 conversion will achieve a similar equilibrium. Indeed, this is the essence of the volcano plot:[36] metals that stabilise hydrides too much or too little are very poor catalysts for H_2 conversion. Nature has positioned [FeFe] hydrogenase at the apex of the volcano plot by selecting the appropriate combination of primary- and secondary-coordination sphere interactions, rivalling precious metals (*e.g.* platinum) in terms of H_2-conversion activity.

PRM thanks Royal Society (RGS\R1\231433), Royal Society of Chemistry (R23-6753486967) and University of Leicester for funding. MTL is supported by a Future 50 Scholarship from University of Leicester. JAB thanks Royal Society (RG\R2\232336), RSC (R22-2594924113), and University of Essex for funding. SM was supported by a Nottingham Research Fellowship from University of Nottingham.

Data availability

Data supporting this article have been included as part of the ESI.†

Conflicts of interest

There are no conflicts to declare.

References

1 S. Singh, *Energy*, 2021, 1–17.
2 A. J. Shih, M. C. O. Monteiro, F. Dattila, D. Pavesi, M. Philips, A. H. M. da Silva, R. E. Vos, K. Ojha, S. Park, O. van der Heijden, G. Marcandalli, A. Goyal, M. Villalba, X. Chen, G. T. K. K. Gunasooriya, I. McCrum, R. Mom, N. López and M. T. M. Koper, *Nat. Rev. Methods Primers*, 2022, **2**, 84.
3 S. Shiva Kumar and V. Himabindu, *Mater. Sci. Energy Technol.*, 2019, **2**, 442–454.
4 S. Wang, A. Lu and C.-J. Zhong, *Nano Convergence*, 2021, **8**, 4.
5 W. Lubitz, H. Ogata, O. Rüdiger and E. Reijerse, *Chem. Rev.*, 2014, **114**, 4081–4148.
6 M. Hambourger, M. Gervaldo, D. Svedruzic, P. W. King, D. Gust, M. Ghirardi, A. L. Moore and T. A. Moore, *J. Am. Chem. Soc.*, 2008, **130**, 2015–2022.
7 Y. Nicolet, A. L. de Lacey, X. Vernède, V. M. Fernandez, E. C. Hatchikian and J. C. Fontecilla-Camps, *J. Am. Chem. Soc.*, 2001, **123**, 1596–1601.
8 Y. Nicolet, C. Piras, P. Legrand, C. E. Hatchikian and J. C. Fontecilla-Camps, *Structure*, 1999, **7**, 13–23.
9 J. W. Peters, W. N. Lanzilotta, B. J. Lemon and L. C. Seefeldt, *Science*, 1998, **282**, 1853–1858.
10 D. W. Stephan, *J. Am. Chem. Soc.*, 2021, **143**, 20002–20014.
11 J. Esselborn, N. Muraki, K. Klein, V. Engelbrecht, N. Metzler-Nolte, U. P. Apfel, E. Hofmann, G. Kurisu and T. Happe, *Chem. Sci.*, 2016, **7**, 959–968.
12 C. Sommer, A. Adamska-Venkatesh, K. Pawlak, J. A. Birrell, O. Rüdiger, E. J. Reijerse and W. Lubitz, *J. Am. Chem. Soc.*, 2017, **139**, 1440–1443.
13 A. Silakov, C. Kamp, E. Reijerse, T. Happe and W. Lubitz, *Biochemistry*, 2009, **48**, 7780–7786.
14 C. Lorent, S. Katz, J. Duan, C. J. Kulka, G. Caserta, C. Teutloff, S. Yadav, U.-P. Apfel, M. Winkler, T. Happe, M. Horch and I. Zebger, *J. Am. Chem. Soc.*, 2020, **142**, 5493–5497.
15 M. Winkler, M. Senger, J. Duan, J. Esselborn, F. Wittkamp, E. Hofmann, U.-P. Apfel, S. T. Stripp and T. Happe, *Nat. Commun.*, 2017, **8**, 16115.
16 D. W. Mulder, Y. Guo, M. W. Ratzloff and P. W. King, *J. Am. Chem. Soc.*, 2017, **139**, 83–86.
17 D. W. Mulder, M. W. Ratzloff, M. Bruschi, C. Greco, E. Koonce, J. W. Peters and P. W. King, *J. Am. Chem. Soc.*, 2014, **136**, 15394–15402.
18 M. T. Lachmann, Z. Duan, P. Rodríguez-Maciá and J. A. Birrell, *Chem. Sci.*, 2024, **15**, 14062–14080.
19 B. M. Hoffman, D. Lukoyanov, Z.-Y. Yang, D. R. Dean and L. C. Seefeldt, *Chem. Rev.*, 2014, **114**, 4041–4062.
20 N. Khadka, R. D. Milton, S. Shaw, D. Lukoyanov, D. R. Dean, S. D. Minteer, S. Raugei, B. M. Hoffman and L. C. Seefeldt, *J. Am. Chem. Soc.*, 2017, **139**, 13518–13524.
21 P. Amara, J.-M. Mouesca, A. Volbeda and J. C. Fontecilla-Camps, *Inorg. Chem.*, 2011, **50**, 1868–1878.
22 P. Knörzer, A. Silakov, C. E. Foster, F. A. Armstrong, W. Lubitz and T. Happe, *J. Biol. Chem.*, 2012, **287**, 1489–1499.
23 G. Berggren, A. Adamska, C. Lambertz, T. R. Simmons, J. Esselborn, M. Atta, S. Gambarelli, J. M. Mouesca, E. Reijerse, W. Lubitz, T. Happe, V. Artero and M. Fontecave, *Nature*, 2013, **499**, 66–69.
24 E. J. Reijerse, C. C. Pham, V. Pelmenschikov, R. Gilbert-Wilson, A. Adamska-Venkatesh, J. F. Siebel, L. B. Gee, Y. Yoda, K. Tamasaku, W. Lubitz, T. B. Rauchfuss and S. P. Cramer, *J. Am. Chem. Soc.*, 2017, **139**, 4306–4309.
25 A. R. Finkelmann, M. T. Stiebritz and M. Reiher, *Chem. Sci.*, 2014, **5**, 215–221.
26 J. H. Artz, O. A. Zadvornyy, D. W. Mulder, S. M. Keable, A. E. Cohen, M. W. Ratzloff, S. G. Williams, B. Ginovska, N. Kumar, J. Song, S. E. McPhillips, C. M. Davidson, A. Y. Lyubimov, N. Pence, G. J. Schut, A. K. Jones, S. M. Soltis, M. W. W. Adams, S. Raugei, P. W. King and J. W. Peters, *J. Am. Chem. Soc.*, 2020, **142**, 1227–1235.
27 J. A. Birrell, V. Pelmenschikov, N. Mishra, H. Wang, Y. Yoda, K. Tamasaku, T. B. Rauchfuss, S. P. Cramer, W. Lubitz and S. DeBeer, *J. Am. Chem. Soc.*, 2020, **142**, 222–232.
28 A. Adamska-Venkatesh, D. Krawietz, J. Siebel, K. Weber, T. Happe, E. Reijerse and W. Lubitz, *J. Am. Chem. Soc.*, 2014, **136**, 11339–11346.
29 S. G. Mayhew, *Eur. J. Biochem.*, 1978, **85**, 535–547.
30 M. A. Martini, O. Rüdiger, N. Breuer, B. Nöring, S. DeBeer, P. Rodríguez-Maciá and J. A. Birrell, *J. Am. Chem. Soc.*, 2021, **143**, 18159–18171.
31 T. Reda, C. D. Barker and J. Hirst, *Biochemistry*, 2008, **47**, 8885–8893.
32 P. Paengnakorn, P. A. Ash, S. Shaw, K. Danyal, T. Chen, D. R. Dean, L. C. Seefeldt and K. A. Vincent, *Chem. Sci.*, 2017, **8**, 1500–1505.
33 K. A. Vincent, G. J. Tilley, N. C. Quammie, I. Streeter, B. K. Burgess, M. R. Cheesman and F. A. Armstrong, *Chem. Commun.*, 2003, 2590–2591.
34 C. Esmieu and G. Berggren, *Dalton Trans.*, 2016, **45**, 19242–19248.
35 J. Esselborn, C. Lambertz, A. Adamska-Venkatesh, T. Simmons, G. Berggren, J. Noth, J. Siebel, A. Hemschemeier, V. Artero, E. Reijerse, M. Fontecave, W. Lubitz and T. Happe, *Nat. Chem. Biol.*, 2013, **9**, 607–609.
36 J. K. Nørskov, T. Bligaard, B. Hvolbæk, F. Abild-Pedersen, I. Chorkendorff and C. H. Christensen, *Chem. Soc. Rev.*, 2008, **37**, 2163–2171.